**Article:**

Lennarz, A., Williams, M., Laird, A. M. orcid.org/0000-0003-0423-363X et al. (16 more authors) (2020) First inverse kinematics measurement of key resonances in the 22Ne(p, γ)23Na reaction at stellar temperatures. Physics Letters B. 135539. ISSN 0370-2693

https://doi.org/10.1016/j.physletb.2020.135539

# First inverse kinematics measurement of key resonances in the $^{22}$Ne$(p,\gamma)^{23}$Na reaction at stellar temperatures

A. Lennarz[a,*], M. Williams[a,b], A. M. Laird[b,c], U. Battino[d,c], A. A. Chen[e], D. Connolly[a,1], B. Davids[a], N. Esker[a,2], R. Garg[b,3], M. Gay[f], U. Greife[g], U. Hager[h], D. Hutcheon[a], J. José[i], M. Lovely[g], S. Lyons[h,j], A. Psaltis[e,c], J. E. Riley[b], A. Tattersall[d], C. Ruiz[a]

[a] *TRIUMF, 4004 Wesbrook Mall, Vancouver, BC, Canada, V6T 2A3*
[b] *Department of Physics, University of York, Heslington, York, UK, YO10 5DD*
[c] *The NuGrid collaboration, http://www.nugridstars.org*
[d] *University of Edinburgh, School of Physics and Astrophysics, Edinburgh EH9 3FD, UK*
[e] *Department of Physics and Astronomy, McMaster University, Hamilton, ON, Canada, L8S 4L8*
[f] *Columbia University, 116th St & Broadway, New York, NY 10027, USA*
[g] *Colorado School of Mines, Golden, CO, USA*
[h] *National Superconducting Cyclotron Laboratory, Michigan State University, East Lansing, MI 48824, USA*
[i] *Departament de Física Universitat Politècnica de Catalunya & Institut d'Estudis Espacials de Catalunya (IEEC), C. Eduard Maristany 10, E-08019 & Ed. Nexus-201, C. Gran Capità, 2-4, E-08034, Barcelona, Spain*
[j] *The Joint Institute for Nuclear Astrophysics–Center for the Evolution of the Elements, Michigan State University, East Lansing, Michigan 48824, USA*

**Abstract**

In this Letter we report on the first inverse kinematics measurement of key resonances in the $^{22}$Ne$(p,\gamma)^{23}$Na reaction which forms part of the NeNa cycle, and is relevant for $^{23}$Na synthesis in asymptotic giant branch (AGB) stars. An anti-correlation in O and Na abundances is seen across all well-studied globular clusters (GC), however, reaction-rate uncertainties limit the precision as to which stellar evolution models can reproduce the observed isotopic abundance patterns. Given the importance of GC observations in testing stellar evolution models and their dependence on NeNa reaction rates, it is critical that the nuclear physics uncertainties on the origin of $^{23}$Na be addressed. We present results of direct strengths measurements of four key resonances in $^{22}$Ne$(p,\gamma)^{23}$Na at $E_{c.m.}$ = 149 keV, 181 keV, 248 keV and 458 keV. The strength of the important $E_{c.m.}$ = 458 keV reference resonance has been determined independently of other resonance strengths for the first time with an associated strength of $\omega\gamma$ = 0.439(22) eV and with higher precision than previously reported. Our result deviates from the two most recently published results obtained from normal kinematics measurements performed by the LENA and LUNA collaborations but is in agreement with earlier measurements. The impact of our rate on the Na-pocket formation in AGB stars and its relation to the O-Na anti-correlation was assessed via network calculations. Further, the effect on isotopic abundances in CO and ONe novae ejecta with respect to pre-solar grains was investigated.

*Keywords:* Inverse Kinematics Measurements, Radiative Capture Reactions, Stellar Nucleosynthesis

## 1. Introduction

Globular clusters (GCs) are dense aggregates of predominantly old stars found in the galactic halo and have long fascinated astronomers for the unique insight they provide into the processes driving galaxy formation and chemical evolution. In particular, GCs are ideal test sites for answering open questions about the interplay between primordial and evolutionary chemical enrichment [1]. These objects have therefore warranted significant observational efforts and, through recent studies a complex picture of GCs abundance patterns has emerged, with strong evidence supporting multiple epochs of star formation [2]. Despite clear variability in observed abundances, some ubiquitous trends become apparent, such as the anti-correlation in oxygen and sodium abundances [3]. Currently stellar models are unable to reproduce many of the abundance patterns present in GC stars along the red-giant branch (RGB), but absent in their field star counterparts [2, 4, 5]. AGB stars undergoing Hot Bottom Burning (HBB) are currently the most favored astrophysical sites to explain the O-Na anti-correlation [6, 7]. HBB occurs during the quiescent phase between two thermal pulses (TP) when part of the H-shell is included in the envelope convection and the H-shell has enhanced access to fuel which is convectively mixed into its outer layers. In TP-AGB stars, sodium is primarily synthesized by proton-capture on $^{22}$Ne in the outer-most layer of the core-envelope transition zone, resulting in the formation of a so-called $^{23}$Na pocket [8, 9]. This pocket forms when $^{22}$Ne and $^{12}$C abundances are comparable, and the $^{22}$Ne$(p,\gamma)^{23}$Na and $^{12}$C$(p,\gamma)^{13}$N reactions compete. In

*Corresponding author
*Email address:* lennarz@triumf.ca (A. Lennarz )

[1] present address: Los Alamos National Laboratory, Los Alamos, New Mexico 87545, USA
[2] present address: San José State University, 1 Washington Square, Duncan Hall 518 San José, CA 95192-0101
[3] present address: University of Edinburgh, School of Physics and Astrophysics, Edinburgh EH9 3FD, UK

low-mass AGB stars, at solar metallicity, models predict the $^{23}$Na pocket to be the main sodium source, and the overproduction of sodium to result from the ingestion of the $^{23}$Na pocket during the thermal dredge up [8]. The $^{22}$Ne$(p,\gamma)^{23}$Na reaction further affects the $^{20}$Ne/$^{22}$Ne, $^{21}$Ne/$^{22}$Ne and $^{20}$Ne/$^{21}$Ne abundance ratios of pre-solar grains found in meteorites. These grains are important signatures of nucleosynthesis in different stellar environments and mixing in stellar ejecta before the formation of our solar system. The $^{22}$Ne$(p,\gamma)^{23}$Na reaction is also influential in nova nucleosynthesis as has been identified by a sensitivity study by Iliadis *et al.*, showing that nuclear uncertainties associated with this reaction rate can significantly influence the final abundances of $^{22}$Ne and $^{23}$Na [10].

In recent years the $^{22}$Ne$(p,\gamma)^{23}$Na reaction has been targeted intensively at three facilities, all employing normal kinematics techniques [11, 12, 13, 14]. The low-energy regime was investigated by the LUNA and LENA collaborations, since the rate is dominated by narrow low-energy resonances. With the exception of the low-energy resonance strength measurements by LUNA [13, 14] with $E_{c.m.} \leq 248$ keV, all previously reported strengths were either measured relative to reference resonances at $E_{c.m.}$ = 458 keV or 1222 keV or depended on these resonances to determine target stoichiometries. The 458 keV resonance strength directly influences the strengths of the low-energy resonances reported by the LENA collaboration [12], and was used as reference for target stoichiometries in $^{22}$Ne+$\alpha$ [15] and normal kinematics studies of the $^{22}$Ne$(p,\gamma)^{23}$Na reaction [11]. Moreover, this resonance is particularly relevant for reaction-rate compilations conducted by Sallaska, Iliadis *et al.* [16], for which all other measured strengths were normalized to the 458 keV strength value of $\omega\gamma$ = 0.524(51) eV [17]. The latter was determined relative to the $E_p$ = 405.5(3) keV ($\omega\gamma = (8.63(52)\times10^{-3})$ eV [18]) resonance strength in $^{27}$Al$(p,\gamma)^{28}$Si, and depends on the background contribution of the $E_p$ = 326 keV and 447 keV resonances in the same reaction. We note that there is a more recent result for the 405.5(3) keV strength of $\omega\gamma = 1.04(5)\times10^{-2}$ eV [19]. Using this value for re-normalization would reduce the 458 keV strength reported by Longland *et al.* to $\omega\gamma$ = 0.435(42) eV. Further, the strengths of the resonances affecting the background in that measurement have also been normalized to the 405.5(3) keV strength. Though the 458 keV resonance has been investigated numerous times [17, 11, 20], our measurement reveals that the situation for its strength is still not resolved. In fact, the strength of this resonance has never been measured independently of other resonances. However, this work puts forward a direct, reference-independent measurement which is largely independent of knowledge of the relevant branching ratios (BRs). This letter further presents the results of the direct strengths measurements of the astrophysically important resonances in $^{22}$Ne$(p,\gamma)^{23}$Na at $E_{c.m.}$ = 149 keV, 181 keV, 248 keV.

## 2. Experimental Details

The measurement was performed using the DRAGON (Detector of Recoil and Gammas Of Nuclear reactions) recoil separator [21] at the ISAC beam facility at TRIUMF, Vancouver, Canada. DRAGON is designed to conduct studies of radiative capture reactions in inverse kinematics and consists of: (1) a windowless, differentially pumped, recirculated gas target surrounded by a high-efficiency $\gamma$-detector array consisting of 30 BGO detectors; (2) a high-suppression electromagnetic mass separator with two stages of charge and mass selection; (3) a variable heavy ion detection system in combination with two micro-channel plate (MCP) based timing detectors for time-of-flight (TOF) measurements. The recoil-detection system consisted of a double-sided silicon strip detector (DSSSD) [21, 22].

A high intensity ($\sim 2 \times 10^{12}$ ions/sec) isotopically pure $^{22}$Ne$^{4+}$ beam was delivered to the hydrogen-filled gas target. $^{23}$Na recoils were transmitted through the separator and detected in the DSSSD. To contain the entire yield profile of the resonances within the target, an average gas pressure of 5 Torr was used ($\sim 3.9\times10^{18}$ hydrogen atoms/cm$^2$). The maximum charge state was selected by transmitting the beam through the magnetic dipoles. Equilibrium charge-state distributions for $^{23}$Na ions in hydrogen were measured at recoil energies to eliminate systematic uncertainties associated with semi-empirical calculations. Two silicon surface barrier detectors positioned at 30° and 57° relative to the beam axis inside the target detected elastically scattered protons for a relative measure of the beam intensity. The elastic scattering rate was normalized to automated hourly Faraday Cup readings. The energy loss across the target was determined by measuring the incoming and outgoing beam energy via the magnetic field of the first magnetic dipole, which centered the beam on-axis. The incoming beam-energy spread was $\sim$0.1% FWHM [23]. Stopping powers were calculated based on the energy loss, the gas density derived from continuously recorded pressure and temperature, and the effective target length [21]. This reduces uncertainties induced by the commonly used software packages SRIM [24] and LISE [25]. The beam heating effect on the measured yield under the experimental conditions, i.e., beam powers, beam energies and gas pressures given in this work has been found to be negligible with a dissipated power of $\sim$0.12 Watts and an average heating of $\sim$0.18 to $\sim$0.24K. For further details on the effect of intense ion beams on gas target densities we refer to Ref. [26]. Resonance energies were determined via the position sensitive BGO array by relating the centroid of the distribution ($\gamma$ yield vs target position) to the incoming and outgoing beam energy [23].

## 3. Analysis

For improved background suppression, the resonance strengths were extracted in a coincidence analysis, where the `GEANT3` [27] simulation used to determine the BGO detection efficiency relies on literature BRs. For the 458 keV measurement the DSSSD energy spectrum was fitted with a double Gaussian to set appropriate energy cuts for the "golden" recoil gate at $\pm 3.5\sigma$ relative to the peak centroids, and to account for the satellite peak at the low energy side of the main recoil peak (Fig. 1). The satellite peak results from the additional energy loss of ions passing the $\sim$3% aluminum DSSSD grid [28]. Accounting for satellite peak and inter-strip events results in a DSSSD efficiency of $(96.15 \pm 0.1_{stat.} \pm 0.43_{sys.})\%$ [29]. The

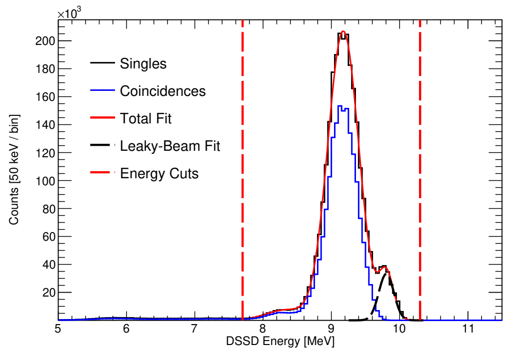


Figure 1: Singles (black histogram) and coincidence (blue histogram) DSSSD energy spectra of the 458 keV yield measurement. In red, the triple Gaussian fit of the singles spectrum is shown. The black dashed line denotes the unreacted beam component (not present in coincidence measurement) of the fit and the red dashed vertical lines indicate the recoil gate.

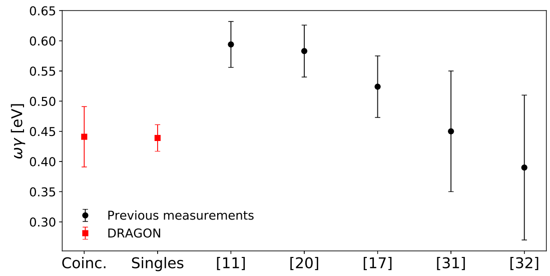


Figure 2: Previous 458 keV strength values (black circles) in relation to the DRAGON results (red squares) obtained from singles and coincidence analysis.

established DSSSD and BGO energy gates were then placed on the separator TOF, i.e., the time between $\gamma$- and recoil event detection, spectrum to extract the number of recoils. The background was estimated by sampling the time-random background and calculating an average expectation over the width of the signal region using a poissonian background model. High statistics and a clear separation of unreacted beam and recoils also allowed for a singles analysis of the 458 keV resonance to eliminate uncertainties introduced by the dependence of the coincidence analysis on BRs and BGO efficiency. Using the fit parameters of the coincidence spectrum as guide for the singles analysis, a triple Gaussian function was applied to the DSSSD energy spectrum, and the integral of the main recoil peak and satellite peak comprises the number of recoil events. Figure 2 presents the 458 keV resonance-strength values based on coincidence and singles analysis, which are mutually consistent, relative to previous measurements.

The resonance strengths were calculated using the standard formula for thick target yield in inverse kinematics [30],

$$\omega\gamma = \frac{2\epsilon Y}{\lambda^2_{c.m.}} \frac{m}{m+M}, \tag{1}$$

with the recoil yield, $Y$, the stopping power in the laboratory system, $\epsilon$, the center-of-mass de-Broglie wavelength, $\lambda^2_{c.m.}$ as well as the proton (m) and $^{22}$Ne (M) masses. Our result for the 458 keV strength of $\omega\gamma_{coinc}$ = 0.441(50) eV ($\omega\gamma_{singles}$ = 0.439(22) eV) is lower and not in agreement within errors with the two latest results [11, 20]. However, it agrees with three previous values [17, 31, 32]. The result from Meyer *et al.* [32] was normalized to the 612 keV resonance strength, and the Endt *et al.* [31] value is based on Ref. [32], however, normalized the 1.222 MeV resonance strength from Ref. [33]. The sensitivity of former studies to reference resonances underlines the necessity of reference-independent measurements as well as more precise measurements of reference-resonance strengths.

To determine the 149 keV, 181 keV and 248 keV resonance strengths, conservative recoil gates for DSSSD and BGO energy were placed on the separator TOF vs MCP TOF spectrum or separator TOF spectrum (Fig. 3). The 248 keV yield measurement does not have an associated separator vs MCP TOF spectrum since the MCP detection efficiency was too low to give enough statistics; this issue was resolved for the lower energy measurements.

For the analysis of the 149 keV and 181 keV yield measurements the branching ratios for the $E_x$ = 8943(3) keV and 8972(3) keV levels given in Ref. [12] were used for the `GEANT3` simulation. The BRs from Ref. [12] were chosen over those reported in Ref. [34] as the analysis in Ref. [12] did not require additional background subtraction or coincidence-summing corrections, and accounted for escape peaks and Compton continuum. To investigate how the choice of BRs propagates to the BGO detection efficiencies and resonance strength, respectively, simulations were performed for both sets of BRs. A difference of 1.1 % and 3.7% in simulated efficiency was found for the 149 keV and 181 keV resonances, respectively, which has been taken into account in the uncertainty budget.

## 4. Results

For the 149 keV resonance we report a strength of $\omega\gamma$(149) = (1.67 ± 0.28 (sys) $^{+0.39}_{-0.28}$ (stat))×10$^{-7}$ eV, which is lower but in agreement with all previous values. Our 181 keV strength of $\omega\gamma$(181) = (2.17$^{+0.32}_{-0.31}$ (sys) $^{+0.2}_{-0.17}$ (stat))×10$^{-6}$ eV is in good agreement with the LUNA HPGe result [14] and lower but also in agreement with the TUNL result. Further, our result is 20% lower than the LUNA BGO measurement [13] (compare Tab. 1), though the two values are still consistent within 1 $\sigma$. Regarding the 248 keV resonance we report a strength of $\omega\gamma$(248) = 8.5(1.4)×10$^{-6}$ eV. The dominant contributions to the systematic uncertainty result from uncertainties on coincidence efficiency (10%), stopping power (4.3 - 5.9%), charge-state fraction (1.8%(181 keV) - 2.4%(149 keV)), MCP efficiency (5%) and beam normalization (1.1 - 4.9%).

In view of the significant deviation of the DRAGON $\omega\gamma$(458 keV) result from the value used to normalize the strengths of the low-energy resonances in the TUNL measurement [12], we carefully reviewed the latter. In fact, renormalizing the TUNL 149 keV strength to our $\omega\gamma$(458 keV) result, brings it into better agreement with DRAGON, and a re-

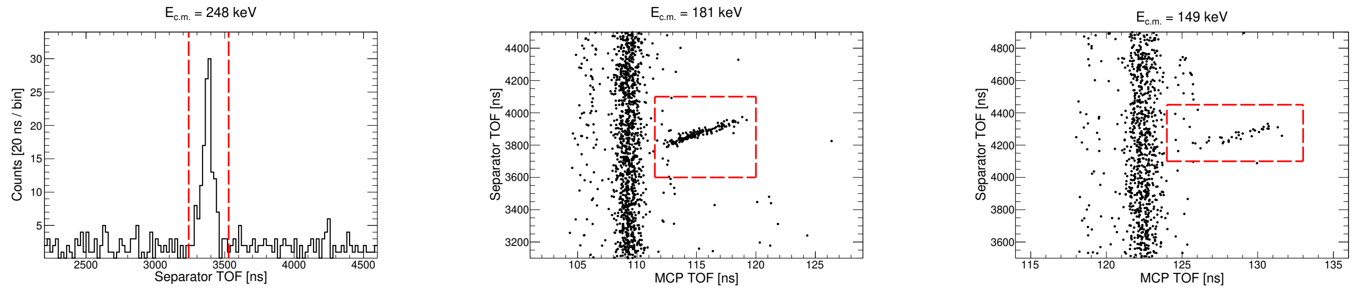


Figure 3: Separator TOF spectrum for the 248 keV resonance, and separator vs MCP TOF spectra for the 181 keV and 149 keV yield measurements. The red dashed lines represent the recoil timing gates. Each spectrum is gated on the recoil peak in the DSSSD energy spectrum and a minimum BGO energy threshold of $E_\gamma >$ 2.2, 2.0, and 2.5 MeV, respectively.

Table 1: Overview of resonance strengths. (S) marks results from a singles analysis.

| $E_{c.m.}$ [keV] | $\omega\gamma$ [eV] | | |
|---|---|---|---|
| | Lit. | This work | |
| 458.0(3) [35] | 0.583(43) [20] | 0.441(50) | 0.439(22) (S) |
| | 0.594(38) [11] | | |
| 248.3(6) [36] | $8.2(7)\times10^{-6}$ [14] | $8.5(1.4)\times10^{-6}$ | |
| | $9.7(7)\times10^{-6}$ [13] | | |
| 181.2(7) [36] | $2.2(2)\times10^{-6}$ [14] | | |
| | $2.7(2)\times10^{-6}$ [13] | $2.17^{+0.37}_{-0.35}\times10^{-6}$ | |
| | $2.32(32)\times10^{-6}$ [12] | | |
| 149.4(7) [36] | $1.8(2)\times10^{-7}$ [14] | | |
| | $2.2(2)\times10^{-7}$ [13] | $1.67^{+0.48}_{-0.40}\times10^{-7}$ | |
| | $2.03(40)\times10^{-7}$ [12] | | |
| | Ref. [12] re-normalized to this work | | |
| 181.2(7) [36] | $1.75(29)\times10^{-6}$ | | |
| 149.4(7) [36] | $1.53(33)\times10^{-7}$ | | |

normalized 181 keV strength is compatible with the DRAGON and LUNA HPGe results.

## 5. Astrophysical Impact

Figure 4 displays an overlay of the rates determined from this work and those of LUNA and TUNL measurements. For the DRAGON reaction rate evaluation, the analysis results from higher energy resonances at 610 keV, 632 keV and 1222 keV as well as the direct-capture contribution as detailed in Ref. [37] were included in addition to the here discussed resonance strengths. The dramatic enhancement of the LUNA rate upper limit is mainly due to the inclusion of the $E_{c.m.}$ = 68 keV resonance, which has been excluded in the median rate and for which only an upper limit has been reported [13]. Our rate maps closely with the TUNL rate, with a slight reduction due to our reduced 149 keV and 181 keV strengths.

The effect of the DRAGON rate compared to the Iliadis 2010 rate [38] on the sodium and neon abundances in neon-oxygen (ONe) novae with underlying white-dwarf (WD) masses of 1.15 $M_\odot$ and 1.25 $M_\odot$, as well as carbon-oxygen (CO) novae (1.15 $M_\odot$ and 1.00 $M_\odot$) was investigated using hydrodynamical nova models [39, 40]. Changes of more than 10% in the isotopic abundances within the Ne-Al region ($^{20,21,22}$Ne, $^{22,23}$Na, $^{25,26}$Mg, $^{26,27}$Al) in 1.15 $M_\odot$ CO novae, and a factor of 2 enhancement in $^{23}$Na abundance are observed for both CO nova mass models. For ONe novae, a factor of 2 reduction of the $^{22}$Ne content is observed for both WD mass models. Further, the $^{24}$Mg abundance is enhanced by ~15% in the 1.25 $M_\odot$ model, whereas only slight differences are seen for the remaining isotopes considered in both models. Regarding CO novae, our rate increases the differences in the $^{25}$Mg/$^{26}$Mg and $^{26}$Mg/$^{25}$Mg ratios between the 1.0 and 1.15 $M_\odot$ models. Using the DRAGON rate in the 1.15 $M_\odot$ model increases the $^{25}$Mg/$^{24}$Mg ratio by 24% and decreases the $^{26}$Mg/$^{25}$Mg ratio by 13% compared to the `STARLIB2013` rate. This can be explained by the sensitivity of Mg synthesis to the peak temperature [41]. Due to the larger rate, the mass flow is pushed up to Mg synthesis temperatures. As a result of this correlation these ratios become relevant in the identification of pre-solar grains, as they function as probe for the peak temperature reached in the outburst, and the underlying WD mass. In a sensitivity study [10], the final abundances of $^{24,25}$Mg for 1.0 $M_\odot$ CO novae varied by up to a factor of 5, when varying the $^{22}$Ne$(p,\gamma)^{23}$Na rate (`STARLIB2013`) within its uncertainties, whereas the DRAGON rate, which as stated above closely maps with the TUNL rate, strongly limits the reaction rate uncertainty in the temperature range of interest ($T_{peak}$ = 170 MK). Varying the new rate within its limits only changes the Mg isotope mass fractions by up to 7% in the 1.15 $M_\odot$ CO nova model. For ONe novae, the cycling back to $^{20}$Ne is irrelevant for both mass models, as $^{20}$Ne is sufficiently available. This is reflected in the same $^{20,21}$Ne final yield, independent of the model. Abundances of $^{23}$Na, $^{24}$Mg or higher mass isotopes remain unaffected. Instead, the observed difference in $^{22}$Ne abundances may be relevant for studies of pre-solar grains. For further details on the impact of the rate from this work on isotopic abundances compared to the `STARLIB2013` rate the reader is referred to Ref. [37].

The NuGrid multi-zone post-processing code MPPNP [42] was used to implement our rate in nucleosynthesis network calculations, and to model the [Na/Fe] abundance ratio on the AGB star surface at the end of the evolution of stable isotopes for various masses and metallicities (compare Fig. 5). A 5 $M_\odot$ model with metallicity z = 0.006 was utilized to study the impact of our rate on HBB in TP-AGB stars, using the `STARLIB2013` rate as reference. We observe a close mapping of [Na/Fe] as a function of [s/Fe] for the two rates, confirming the robustness of the `STARLIB2013` rate. This contradicts the fac-

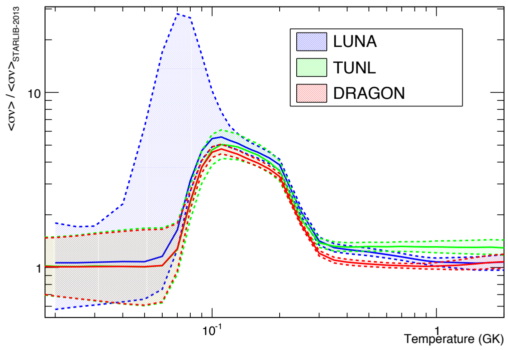


Figure 4: The $^{22}$Ne$(p,\gamma)^{23}$Na reaction rate normalized to the `STARLIB2013` rate [16]. Shaded areas bound the $1-\sigma$ upper and lower limits of each calculated rate. The DRAGON rate was calculated using the same `RateMC` code [38] used for the TUNL rate.

tor of ~3 enhancement in $^{23}$Na production for 5 $M_\odot$ AGB stars stated by Slemer *et. al.* [43] based on the LUNA rate, which includes the tentative $E_{c.m.}$ = 68 keV and 100 keV resonances. Even though Slemer *et. al.* use a code that couples mixing and burning during HBB, and adopt a similar list of isotopes as NuGrid, neutron captures are not included. Thus, the important $^{23}$Na destruction channel $^{23}$Na$(n,\gamma)^{24}$Na stated in Ref. [44] remains unconsidered. Further, the effect of the $^{22}$Ne$(p,\gamma)^{23}$Na rate on the sodium abundance was studied. When closing the (p,$\gamma$) channel, the abundance drops to almost zero, confirming the $^{22}$Ne$(p,\gamma)^{23}$Na reaction as main sodium production channel in massive AGB stars. Further, the effect on the $^{23}$Na-pocket in low-mass AGB stars (2$M_\odot$, z = 0.001 and z = 0.006) formed with the DRAGON rate relative to the `STARLIB2013` rate was investigated by evaluating the abundance profile of $^{23}$Na when the sodium pocket is fully formed (Fig. 5). Switching off the $^{22}$Ne$(p,\gamma)^{23}$Na reaction results in a significant abundance reduction. However, in contrast to the 5 $M_\odot$ model, the sodium abundance stays relatively high due to the second production channel $^{22}$Ne(n,$\gamma$)$^{23}$Ne($\beta^-$)$^{23}$Na, which is active during radiative $^{13}$C burning as well as during convective $^{22}$Ne burning [44].

## 6. Summary

In summary, key resonances in the $^{22}$Ne$(p,\gamma)^{23}$Na reaction have been investigated in inverse kinematics for the first time using the DRAGON recoil separator. The strength of the important reference resonance at 458 keV has been determined more precisely via a direct measurement, and does not agree within errors with the two most recent normal kinematics results. Our result affects resonance strengths that have been determined relative to the strength of this resonance, as well as neon-target stoichiometries determined based on its strength. A new reaction rate was calculated based on the DRAGON measurement, which confirms the accuracy of the current $^{23}$Na production results in AGB stars in relation to the behavior of the $^{22}$Ne$(p,\gamma)^{23}$Na reaction and underlines the importance of this reaction for the sodium production in AGB stars. Further work

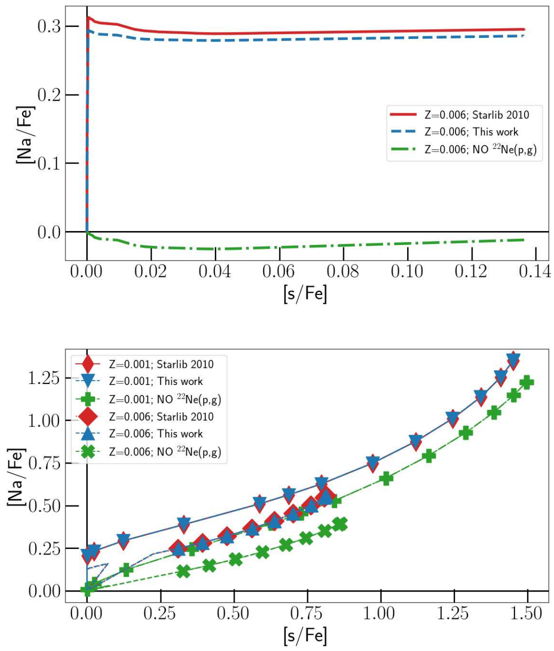


Figure 5: Predicted surface [Na/Fe] abundance ratio as a function of *s* process element abundances [s/Fe] for a 5$M_\odot$ (top) at z = 0.006 and a 2$M_\odot$ (bottom) AGB star model at different metallicities (z = 0.001 and z = 0.006) using the rate from this work relative to the STARLIB rate.

is needed to reassess the sensitivity of Mg isotopic ratios in CO novae to rate variations in the Ne-Al region to use said ratios as a probe of the underlying WD peak temperatures.

## 7. Acknowledgements

The authors thank the ISAC operations and technical staff at TRIUMF. TRIUMF's core operations are supported via a contribution from the federal government through the National Research Council Canada, and the Government of British Columbia provides building capital funds. DRAGON is supported by funds from the National Sciences and Engineering Research Council of Canada. The authors acknowledge support from the "ChETEC" COST Action (CA16117), supported by COST 116 (European Cooperation in Science and Technology). MW, AML, JR were supported by the UK Science and Technology Facilities Council (STFC). UB acknowledges support from the European Research Council ERC-2015-STG Nr. 677497. J. José acknowledges support from the Spanish MINECO grant AYA2017-86274-P, the EU FEDER funds and the AGAUR/Generalitat de Catalunya grant SGR-661/2017. Authors from the Colorado Scool of Mines acknowledge funding via the U.S. Department of Energy grant DE-FG02-93ER40789. The authors also thank R. Longland for his support in calculating the thermonuclear reaction rate presented in this work.

## References

[1] R. Gratton, C. Sneden, E. Carretta, Annu. Rev. Astron. Astrophys. **42** (2004) 385–440.

[2] R. G. Gratton, E. Carretta, A. Bragaglia, Astron. Astrophys. Rev. **20** (2012) 50.
[3] E. Carretta, A. Bragaglia, R.-G. Gratton, et al., Astron. & Astrophys. **450** (2006) 523–533.
[4] E. Carretta, A. Bragaglia, R.-G. Gratton, S. Lucatello, G. Catanzaro, F. Leone, M. Bellazzini, R. Claudi, V. D'Orazi, et al., Astron. & Astrophys. **505** (2009) 117–138.
[5] E. Carretta, A. Bragaglia, R.-G. Gratton, S. Lucatello, Astron. & Astrophys. **505** (2009) 139–155.
[6] A. Renzini, Mon. Not. R. Astron. Soc. **391** (2008) 354–362.
[7] J.-W. Lee, Mon. Not. R. Astron. Soc.: Lett. **405** (2010) L36–L40.
[8] S. Cristallo, O. Straniero, R. Gallino, et al., Astrophys. J. **696** (2009) 797–820.
[9] S. Lucatello, T. Masseron, J. A. Johnson, et al., Astrophys. J. **729:40** (2011) 13pp.
[10] C. Iliadis, A. Champagne, J. José, S. Starrfield, P. Tupper, Astrophys. J. Suppl. S. **142** (2002) 105.
[11] R. Depalo, F. Cavanna, F. Ferraro, et al., Phys. Rev. C **92** (2015) 045807.
[12] K. J. Kelly, A. E. Champagne, L. N. Downen, J. R. Dermigny, S. Hunt, C. Iliadis, A. L. Cooper, Phys. Rev. C **95** (2017) 015806.
[13] F. Ferraro, M. P. Takács, D. Piatti, F. Cavanna, R. Depalo, M. Aliotta, D. Bemmerer, A. Best, A. Boeltzig, et al., Phys. Rev. Lett. **121** (2018) 172701.
[14] F. Cavanna, R. Depalo, M. Aliotta, M. Anders, D. Bemmerer, A. Best, A. Boeltzig, C. Broggini, C. G. Bruno, et al., Phys. Rev. Lett. **120** (2018) 239901(E).
[15] U. Giesen, C. P. Browne, J. Görres, S. Graff, C. Iliadis, et al., Nucl. Phys. A **561** (1993) 95.
[16] A. L. Sallaska, C. Iliadis, A. E. Champange, S. Goriely, S. Starrfield, F. X. Timmes, Astrophys. J. Suppl. S. **207** (2013).
[17] R. Longland, C. Iliadis, J. M. Cesaratto, A. E. Champagne, S. Daigle, J. R. Newton, R. Fitzgerald, Phys. Rev. C **81** (2010) 055804.
[18] D. C. Powell, C. Iliadis, A. E. Champagne, et al., Nucl. Phys. A **644** (1998) 263.
[19] S. Harissopulos, C. Chronidou, K. Spyrou, et al., Eur. Phys. J. A. **9** (2000) 479–489.
[20] K. J. Kelly, A. E. Champagne, R. Longland, M. Q. Buckner, Phys. Rev. C **92** (2015) 035805.
[21] D. Hutcheon, S. Bishop, L. Buchmann, M. Chatterjee, A. Chen, et al., Nucl. Instr. & Methods Phys. Res. Sect. A **498** (2003) 190 – 210.
[22] C. Vockenhuber, et al., Nucl. Instr. Meth. in Phys. Res. B **266** (2008) 4167.
[23] D. A. Hutcheon, C. Ruiz, J. Fallis, et al., Nucl. Instr. & Methods Phys. Res. Sect. A **689** (2012) 70–74.
[24] J. F. Ziegler, M. D. Ziegler, P. Biersack, Nucl. Instr. & Methods Res. Sect. B **268** (2010) 1818–1823.
[25] M. P. Kuchera, O. B. Tarasov, D. Bazin, B. Sherril, K. V. Tarasova, J. Phys. Conf. Ser. **664** (2015) 072029.
[26] J. Görres, K. U. Kettner, H. Krawinkel, C. Rolfs, Nucl. Instr. & Methods **177** (1980) 295–303.
[27] R. Brun, F. Bruyant, M. Maire, A. C. McPherson, P. Zanarini, Geant3, CERN-DD-EE-84-1 (1987).
[28] Micron Semiconductor Ltd, micronsemiconductor.co.uk, 2017.
[29] C. Wrede, A. Hussein, J. G. Rogers, J. D'Auria, Nucl. Instr. & Methods Res. Sect. B **204** (2003) 619–624.
[30] C. Rolfs, W. Rodney, Theoretical Astrophysics, University of Chicago Press., 1988.
[31] P. M. Endt, Nucl. Phys. A **521** (1990) 1.
[32] M. A. Meyer, J. J. A. Smit, Nucl. Phys. A **205** (1973) 177.
[33] J. Keinonen, M. Riihonen, A. Anttila, Phys. Rev. C **15** (1977) 579.
[34] R. Depalo, F. Cavanna, M. Aliotta, M. Anders, , D. Bemmerer, A. Best, A. Boeltzig, C. Broggini, C. G. Bruno, et al., Phys. Rev. C **94** (2016) 055804.
[35] R. Firestone, Nucl. Data Sheets **108** (2006) 1–78.
[36] F. Cavanna, R. Depalo, M. Aliotta, M. Anders, D. Bemmerer, A. Best, A. Boeltzig, C. Broggini, C. G. Bruno, et al., Phys. Rev. Lett. **115** (2015) 252501.
[37] M. Williams, A. Lennarz, A. M. Laird, U. Battino, J. José, et al., in preparation (2020).
[38] C. Iliadis, Longland, C. R., A. E., A. Coc, Nucl. Phys. A **841** (2010) 251–322.
[39] J. José, M. Hernanz, Astrophys. J. **494** (1998) 680.
[40] J. José, *Stellar Explosions: Hydrodynamics and Nucleosynthesis* (Boca Raton: CRC Press, FL 2016).
[41] J. José, M. Hernanz, S. Amari, K. Lodders, E. Zinner, Astrophys. J. **612** (2004) 414.
[42] C. Ritter, F. Herwig, S. Jones, M. Pignatari, C. Fryer, R. Hirschi, Mon. Not. R. Astro. Soc. **480** (2018) 538–571.
[43] A. Slemer, P. Marigo, D. Piatti, M. Aliotta, D. Bemmerer, et al., Month. Not. R. Astron. Soc. **465** (2017) 4817 – 4837.
[44] S. Cristallo, R. Gallino, O. Straniero, L. Piersanti, I. Dominguez, Mem. Soc. Astron. Ital. **774** (2006) 77.